Chapter 2

Where we are today: Tomosynthesis research and development

Contents

For many centuries physicians wished for a method to look inside patient without the need for a surgical intervention. The level of recognition of human diseases would have greatly increased if there was a way to make a human body "transparent". Nobody could have even imagined that this dream can come true. With the discovery of X-rays by Wilhelm Conrad Röntgen in 1895 (Roentgen 1895a, Roentgen 1895b) it became possible.

Nowadays, X-ray based imaging techniques include a variety of implementations and applications. Computed radiography (CR)and digital radiography (DR)are used for planar imaging when a three-dimensional object is mapped onto a two-dimensional plane. Variations of computed tomography (CT), such as clinical CT, C-arm, tomosynthesis, micro-CT and industrial CT are used to "cut" an object into a stack of tomographic slices. These X-ray based imaging methods are widely used not only for diagnostics and assistance in clinical practice but also for screening in security applications and for non-destructive material testing in industry, archeology and material sciences.

Y. Levakhina, *Three-Dimensional Digital Tomosynthesis,* Aktuelle Forschung Medizintechnik, DOI 10.1007/978-3-658-05697-1_2, © Springer Fachmedien Wiesbaden 2014

The aim of this chapter is to give an introduction into a modern X-ray based imaging technique, called digital tomosynthesis (DT). First, the basic principles will be explained. Second, a historical overview of the imaging principle and the reconstruction algorithms will be given. Afterwards, a comparison of state-of-the-art devices will be presented. Finally, the theoretical aspects of DT will be discussed and open questions and problems will be summarized.

2.1 Tomosynthesis basics

The basics of the tomosynthesis imaging technique will be given in this section.

2.1.1 Introduction

DT is an X-ray based tomographic imaging technique. It is a non-invasive and non-destructive method for the three-dimensional visualization of the inner structures of an object. DT is known as an attractive low-dose alternative to CT in medical and non-medical imaging applications, when the data acquisition over the full angular range is impossible or infeasible if object is too large or if only a small part of the object is of interest. The primary application of DT is the screening for breast cancer. Here it is used together with traditional mammography for the detection of microcalcifications and tumors (Niklason 1997, Park 2007, Baker 2011). Further medical application fields include pulmonary nodules detection in chest imaging (e.g. Dobbins 2008, Tingberg 2010), dental imaging (Ogawa 2010) and musculoskeletal imaging of hands (Duryea 2003). Non-medical applications of tomosynthesis include security luggage screening in airports (Reid 2011) and non-destructive material testing in industrial imaging (Huang 2004).

A DT data acquisition includes measuring a limited number of low-dose two-dimensional projections of an object. This is done by moving a detector and/or an X-ray tube around the object within a limited angular range. Each measured two-dimensional *intensity* image $I(\mathbf{u}, \theta)$ represents the decreased signal. The decrease is caused by photon-matter interactions (photoelectric absorption, scatter). If no object is present, the initial intensity I_0 will be measured. The model of tomosynthesis measurements is based on the Beer-Lambert absorption law for a polyenergetic spectrum of the X-ray tube and additionally includes a scatter term $r(\mathbf{u}, \theta)$ and the detector efficiency $\varepsilon(E)$

$$I(\mathbf{u}, \theta) = \int_{E_{max}} \varepsilon(E) I_0(E)\, e^{-\int_L \mu(\mathbf{x}, E) d\mathbf{x}} dE + r(\mathbf{u}, \theta). \tag{2.1}$$

Here, L is a path through the object, depending on the direction of the beam θ, $\mathbf{u}$ is a vector describing a point on the detector and $\mu(\mathbf{x}, E)$ is the distribution of X-ray

attenuation coefficients (measured in cm^{-1}) in dependency of position $\mathbf{x}$ within the imaged volume and the energy E (measured in kilo electron volts keV). For simplicity, the scatter term and the detector efficiency term are usually not taken into account. As a further simplification, it can be assumed that the X-ray spectrum is a monoenergetic spectrum. Thus, the dependency of μ on the energy can be omitted. The resulting model is the well known exponential Beer-Lambert law for a monoenergetic spectrum

$$I(\mathbf{u}, \theta) = I_0 e^{-\int_L \mu(\mathbf{x}) d\mathbf{x}}. \tag{2.2}$$

A *projection* image $p(\mathbf{u}, \theta)$ has a linear relation to the attenuation coefficients $\mu(\mathbf{x})$ and is defined as the log-transform

$$p(\mathbf{u}, \theta) = -log\left(\frac{I(\mathbf{u}, \theta)}{I_0}\right) = \int_L \mu(\mathbf{x})\, d\mathbf{x}. \tag{2.3}$$

Two exemplary images of a hand measured using a medical tomosynthesis device are shown in Fig. 2.1a (intensity image) and Fig. 2.1b (projection image). Tomosynthesis projection images can also be post-processed for a better visual perception (see Fig. 2.1c).

The task of DT is to reconstruct an unknown distribution of X-ray attenuation coefficients $\mu(\mathbf{x})$ within the imaged object based on the limited set of measured line integrals $p(\mathbf{u}, \theta)$, i.e. to solve an ill-posed inverse problem. Depending on the type of reconstruction algorithm, either intensity images or projection images are used for reconstruction. In DT the reconstructed slices are typically parallel to the detector, see Fig 2.2a and Fig. 2.2b. Reconstructed tomosynthesis slices of an apple and of a hand at different heights are shown in Fig. 2.2c-Fig. 2.2h. Three reconstructed slices of an apple at 20 mm, 30 mm and 40 mm heights show different cuts through the seeds of the apple. The reconstructed slices of the hand show that different regions of bone are sharp at different heights (marked by ellipses). Regions with distal phalanges are shown at 10 mm. A region with proximal phalanges and a region with carpal bones are shown at 20 mm and a region with metacarpal bones is shown at 28 mm.

Reconstructed images show that despite the fact that a tomosynthesis dataset consists only of a limited number of projections acquired over a limited angular range, the reconstruction of structures at their correct geometrical location is possible.

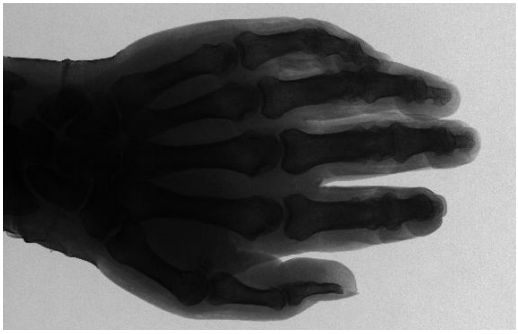

(a) intensity image

(b) projection image

(c) processed projection image for better visual perception

Figure 2.1: Tomosynthesis raw-data of a hand acquired using Siemens Mammomat Inspiration device. (a) intensity image; (b) projection image; (c) post-processed projection image for better visual perception.

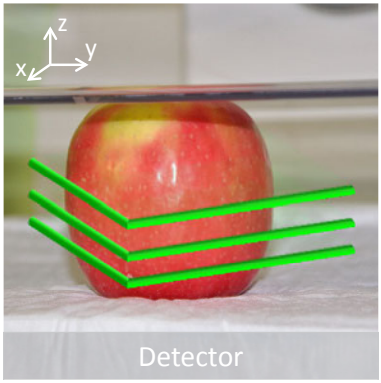

(a) apple, slices orientation

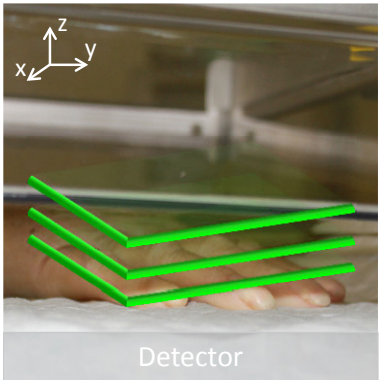

(b) hand, slices orientation

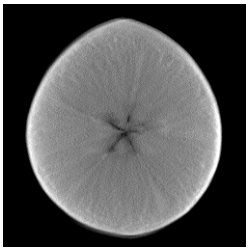

(c) apple, slice at 20 mm

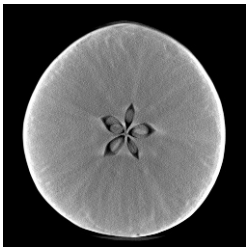

(d) apple, slice at 30 mm

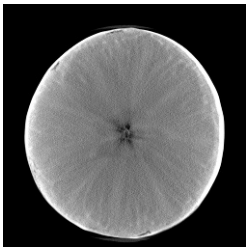

(e) apple, slice at 40 mm

(f) hand, slice at 10 mm

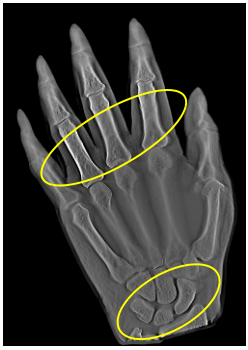

(g) hand, slice at 20 mm

(h) hand, slice at 28 mm

Figure 2.2: Orientation of slices in tomosynthesis (a-b) and tomosynthesis reconstruction results of an apple (c-e) and a hand (f-h). The total height of the apple is 60 mm (60 slices). The total height of the hand is 35 mm (35 slices). Slices at different heights show different (anatomical) structures.

2.1.2 Tomosynthesis technology

2.1.2.1 Acquisition geometry

A tomosynthesis device typically consists of an X-ray tube and a flat-panel detector. During a tomosynthesis acquisition they are moved along a pre-defined trajectory. Several types of motion are possible: a parallel path, a full and a partial isocentric and a circular geometry. In the linear path geometry (Fig. 2.3a) the X-ray tube and the detector are synchronously moved along a line in opposite directions. This geometry corresponds historically to the analogue conventional geometric tomography, see e.g. (Ziedses des Plantes 1932). In the full isocentric geometry (Fig. 2.3b) the X-ray tube and the detector are moved along an arc trajectory around a common origin. If the tube and the detector are moved over 360^o, this geometry describes a cone-beam tomographic system. In the partial isocentric geometry the X-ray tube is moved along an arc while the detector is moved along a line (Fig. 2.3c) or stays fixed (Fig. 2.3d). The partial isocentric geometry with the fixed detector is typically used for breast imaging. In the circular geometry (Fig. 2.3e) the tube and the detector are moved in parallel planes along a circular trajectory. Such a geometry is also known from early works on tomosynthesis (Grant 1972) and is nowadays used in industrial applications. More information about geometries of motion in tomosynthesis can be found e.g. in the review paper by J. T. Dobbins (Dobbins 2003).

2.1.2.2 Geometry parameters

The tomosynthesis geometry parameters include the angular range, the number of projections and the angular step size (a projection density). Parameters for the geometry with a fixed detector and an X-ray tube moving along an arc trajectory are shown schematically in Fig. 2.3f. The *angular range* of the X-ray tube rotation or the *sweep angle* is denoted by θ. In case of a partial isocenter geometry it is defined as the size of the total arc around the rotation center and is described by the X-ray tube position from the first measured projection to the last measured projection. In case of a circular trajectory it is defined as a two-dimensional angle in a three-dimensional space (solid angle) drawn by the X-ray tube. The angular range in clinical applications is typically between 20^o and 50^o. The *number of projections*, denoted by N_{proj}, is the number of measured X-ray images acquired over the angular range θ. The number of projections in clinical applications is typically between 10 and 30. The *angular step size*, denoted by $\Delta\theta$, is defined as the total angular range divided by the number of projections and is described as the angle between the current and the next position of the X-ray tube. Sometimes an inverse measure, called the *projection density*, can be found in

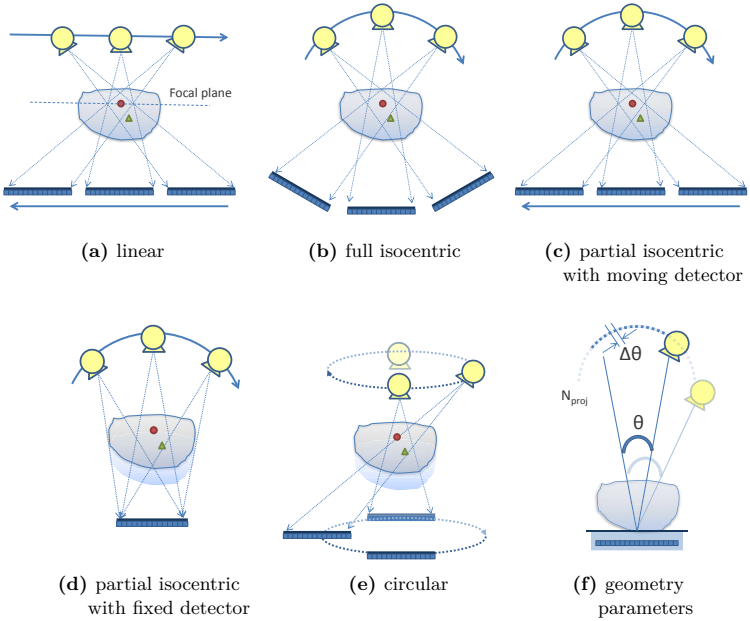

(a) linear **(b)** full isocentric **(c)** partial isocentric with moving detector

(d) partial isocentric with fixed detector **(e)** circular **(f)** geometry parameters

Figure 2.3: (a)-(e) Tomosynthesis geometries; (f) a schematic illustration of parameters for a device with a fixed detector and an X-ray tube moving along an arc trajectory. The following parameters are shown: the angular range θ, number of projections N_{proj} and the angular step $\Delta\theta$.

the literature (Deller 2007, Machida 2010). The projection density is the number of projections divided by the angular range. Another parameter, which is not directly related to the technical parameters of the device but can be seen as a geometry parameter, is the object orientation in the detector xy-plane. It plays an important role and influences the image quality (Cordes 2011, Cordes 2012a, Cordes 2012b, Cordes 2013).

2.1.3 DICOM format

The Digital Imaging and Communications in Medicine (DICOM) standard is a global information-technology standard created by the National Electrical Manufacturers Association (NEMA). DICOM is used for distributing and viewing any kind of medical images worldwide (webNEMA 2013). A DICOM file contains the image data and additionally a file header with supplementary information on the patient, the study,

the device, the physician and the image. There is a number of free DICOM viewers available to open DICOM files, visualize two-dimensional and three-dimensional data and read the header information, among them are ImageJ, Sante DICOM viewer and Agnosco DICOM Viewer. The interested reader can refer, e.g. to the web-page of Chris Rorden (Rorden, C. 2013) for a list of links to free DICOM viewers. There are three build-in MATLAB® commands to read and to save DICOM data and DICOM header automatically: `dicomread`, `dicominfo` and `dicomwrite`.

Typically, the tomosynthesis raw-data and reconstructed images can be exported as a set of DICOM files. If tomosynthesis raw-data are available as DICOM, all necessary information for simulation and reconstruction can be found in the header, see Table 2.1. A DICOM header is comprised of DICOM elements. A DICOM element has a tag, a data type, a length and a value. The tag uniquely defines the properties of an element. It consists of two groups of four digits (sometimes letters), separated by comma and called a Group and an Element. Each attribute has also a name. Typically attribute names are self explaining. A lookup table with the explanation of DICOM attribute names and the corresponding tag numbers can be found, e.g. at (webDICOMLOOKUP 2013). According to the table, e.g. the tag (0018,1110) has the attribute name Distance Source to Detector and denotes the distance in mm from the source to the detector center.

Table 2.1: Important tomosynthesis-related DICOM tags.

Tag	Attribute name
(0018,0050)	Slice Thickness
(0018,11A0)	Body Part Thickness (object height)
(0018,1110)	Distance Source to Detector
(0018,1111)	Distance Source to Patient
(0018,1530)	Detector Primary Angle (X-ray tube angle)
(0018,7026)	Detector Active Dimension(s)
(0028, 0010)	Rows (detector)
(0028, 0011)	Columns (detector)

2.2 From radiostereoscopy to digital tomosynthesis

The principle of *stereoscopy* has been proposed even before the discovery of X-rays. In 1838 Sir Charles Wheatstone demonstrated the physics of binocular vision and proposed a novel device which he called a stereoscope (Wheatstone 1838). The device was designed to present two images with a slight angular offset separately to the left

and the right eye of an observer and by this to create a three-dimensional impression of the presented scene. Moreover, Sir Wheatstone also mentioned in his paper that the discussion on the different visual impression of an object itself and a painting of this object can be already found in the Trattato della Pittura (Treasure of Paining, 1721) of Leonardo da Vinci. The stereoscopy principle was used in the very early development of radiology applications (e.g. Thomson 1896). Apparently, one can draw a connection between the stereoscopy and modern tomosynthesis imaging principle.

The actual history of X-ray imaging starts in 1985 when Wilhelm Conrad Röntgen discovered a new kind of radiation which he called "X-rays" (Roentgen 1895a, Roentgen 1895b). It was a breakthrough invention, which made possible the visualization of inner details of a human body without a surgical intervention. Already shortly after the discovery of X-rays, the harmful effect of ionizing radiation was observed, which cause radiation injury (Upton 1992). Despite all the risks, the X-ray imaging still offers very attractive opportunities.

A simple radiograph contains the superposition of all three-dimensional structures in an object as a two-dimensional shadow. As a consequence, it is impossible to recover the information from which exact three-dimensional position any particular feature (e.g. tumor) originates. In the beginning of the 1920s there were many attempts to erase superimposed shadows from X-ray images and to benefit from the use of X-rays for imaging of the human body. This resulted in a number of patent applications, e.g. in 1922 from the French scientist A. E. M. Bocage (Bocage 1822) and in 1927 from the German scientist E. Pohl (Pohl 1927). A work from the Franco-American technologist J. Kieffer (Kieffer 1929) was also patented and later was commercialized. Besides patents, there was also a number of papers published, among them e.g. in 1914 by the Polish scientist K. Mayer (Mayer 1916), in 1930 by the Italian scientist A. Vallebona (Vallebona 1932) and in 1932 by the Dutch engineer B. G. Ziedses des Plantes (Ziedses des Plantes 1932). Owing to the fact that the communication between researchers from different countries was very limited at that time, all those scientists rediscovered similar concepts. As a summary, all those works deal with the same imaging technique, in which the X-ray tube and the detector are moved in two parallel planes. The goal was to display the plane in focus very sharp and to blur the planes that are out of focus. This technique became known under several names: it was called a *stratigrafia* by A. Vallebona, a *laminography* by J. Kieffer and a *planigraphy* by A. E. M. Bocage and B. G. Ziedses des Plantes. In 1935 G. Grossmann presented a device which he called a *tomograph* (Grossmann 1935a, Grossmann 1935b). It should be noted that the Grossmann's tomograph had nothing to do with the modern tomographic devices but it was also based on the abovementioned principle. More information can be found e.g. in

the historical article written by the curator of the Belgian Museum of Radiology R. van Tiggelen (Van Tiggelen 2002).

The next evolutionary step was the implementation of a device, that enabled the storage of each measured radiograph as a set of separate analogue images. The stored images were processed after the examination instead of doing an integration of measurements directly on the film. Using a set of measured radiographs, it is possible to generate an arbitrary number of planes (Garrison 1969) or laminograms (Miller 1971) through the object. The total radiation dose can thus be reduced because

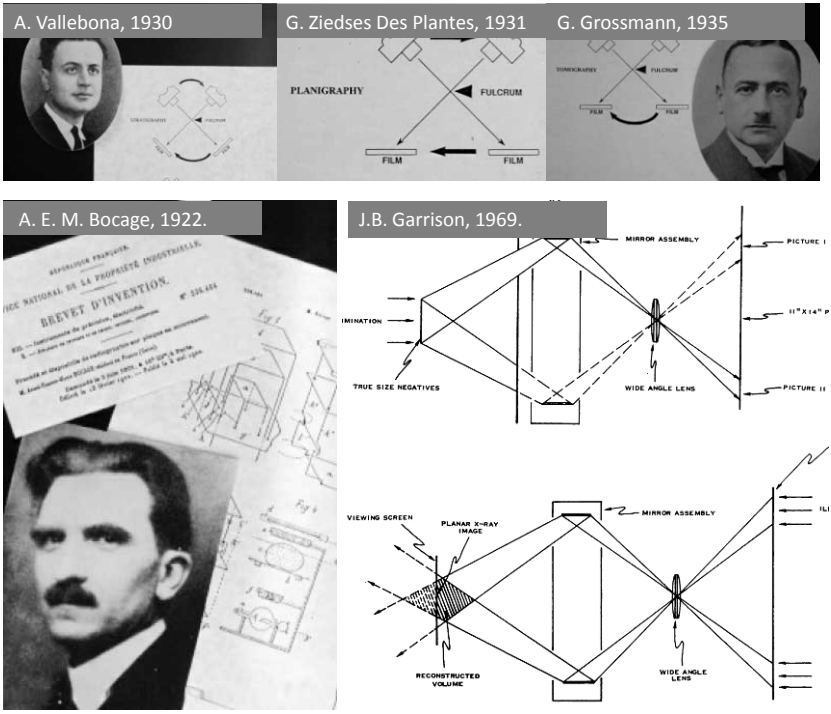

Figure 2.4: A photo collage showing photos of A. E. M. Bocade, G. Ziedses des Plantes, A. Vallebona, G. Grossmann and sketches of early works on tomosynthesis. (Photos courtesy of R. van Tiggelen. Schematical illustrations from (Garrison 1969) are reprinted with permission from the American Journal of Roentgenography.)

Table 2.3: Technical parameters of the Siemens Somatom Definition clinical CT device, the Skyscan 1172 Micro-CT device and the Siemens Mammomat Inspiration DT device.

Parameter	CT	Micro-CT	Tomosynthesis
Angular range θ / deg	360	360	± 25
Angular step size $\Delta\theta$ / deg	0.3	0.3-0.9	2
Number of projections N_{proj}	> 1000	> 1000	25
Acquisition time / sec	0.1-1	> 3600	30
X-ray tube	small cone angle	cone-beam	half-cone
Trajectory	spiral	circle	arc
Voltage / kV	140	20-100	≤ 35
Filter	-	Al, Cu, Al+Cu, selected by user	Rhodium (0.05 mm)
Current / mA	100-500	20-100	100-500
Detector type	curved, multi-row	flat-panel	flat-panel
Detector size / mm	2400	54×22	240×300
Detector element size / mm	3	0.022	0.085
Detector size / pix	$(736 \times 2) \times 16$	1280×1280	3584×2816
Raw-data / GB	> 1	> 0.5	0.5

Table 2.4: Reconstruction parameters of the Siemens Somatom Definition clinical CT device, the Skyscan 1172 Micro-CT device and the Siemens Mammomat Inspiration DT device.

Parameter	CT	Micro-CT	Tomosynthesis
Object size / mm	human body	$4 \times 4 \times 4$	$200 \times 300 \times 100$
Number of images (slices)	> 1000	> 1000	30-100
Image size / pixels	512×512	1280×1280	3584×2816
Slice thicknes / mm	0.6	0.02	1
Voxel size / mm	$0.6 \times 0.6 \times 0.6$	$0.02 \times 0.02 \times 0.02$	$0.085 \times 0.085 \times 1$
Resolution	isotropic	isotropic	non-isotropic, limited in-depth
Image orientation	perpendicular to the detector	perpendicular to the detector	parallel to the detector
Reconstruction time / sec	real time	> 3600	60
Reconstruction / GB	0.1-1	1-10	> 0.8

2.5 Problems of limited data tomography

A tomosynthesis data acquisition results in an incomplete dataset. In this section several theoretical aspects of image reconstruction in case of limited data will be discussed.

The tomographic reconstruction problem can be formulated as follows. Let Ω denote the support of the object (the set of points over which it is nonzero). The non-negative function μ describes the X-ray attenuation coefficients and is zero outside Ω. If an ideal infinitely thin monoenergetic X-ray beam with initial intensity I_0 passes through the object along a straight line l, then the measured intensity I after passing the object will be

$$I = I_0 e^{-\int_l \mu(s)ds}. \tag{2.5}$$

If we define $f_L = -ln\,(I/I_0)$ and assume that L is the set of all lines in Ω, then

$$f_L = \int_L \mu\,(s)\,ds, \tag{2.6}$$

where s denotes a measure along L. The reconstruction problem is to recover the unknown function μ based on the set of line integrals f_L (Radon 1917, Cormack 1963, Cormack 1964).

2.5.1 Types of limited data problems

Four types of limited data problems exist, according to the classification by T. Quinto (Quinto 2012).

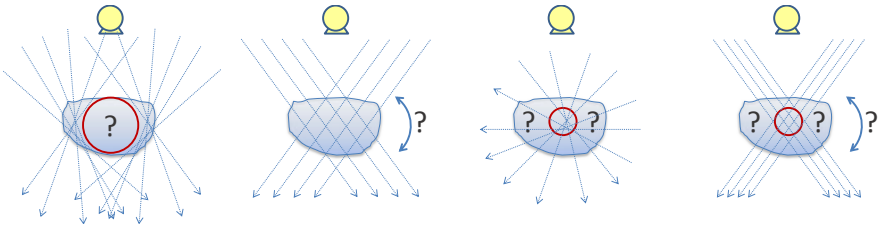

(a) exterior CT **(b)** limited angle **(c)** ROI CT **(d)** limited angle ROI CT

Figure 2.12: Types of limited data according to T. Quinto (Quinto 2012).

The first type is called the *exterior CT* problem (Fig. 2.12a). Here, only the data outside an excluded region (marked by a circle) are measured. The task is to recover the

object outside this region. The second type is called the *limited angle CT* (Fig. 2.12b). Only the data within a limited angular range are available. A unique solution exists but it is very unstable. The third type is called the *ROI CT*, where measurements are done within a limited region of interest (marked by a circle). Because of the overlapping principle of the CT measurements, also the contribution from the object outside the ROI is included into the measured data. Nevertheless, only the reconstruction of the selected region of interest is required (Fig. 2.12c). No unique solution exists (Noninjectivity Theorem). The fourth type is called the *limited angle ROI CT*. It is a combination of the second and the third type (Fig. 2.12d). The tomosynthesis problem can be classified as the second type of limited data problem.

2.5.2 Radon transform and singularities

The Radon transform is the most important transform in the mathematical theory of tomography. Johann Radon proposed a mathematical technique how to determine a function based on its line integrals in 1917 (Radon 1917). This paper was later translated to English (Radon 1986). Allan M. Cormack independently studied the same problem and published two papers in 1963 and 1964 (Cormack 1963, Cormack 1964). As he mentioned in the Nobel lecture (Cormack 1979), he learned only fourteen years later that Radon already had solved this problem in 1917.

Let a direction vector θ belong to a unit sphere $\theta \in S^{n-1}$ and $\Theta^{\perp} = \{t\theta^{\perp} : t \in \mathbb{R}\}$ be a hyperplane through the origin perpendicular to θ. The Radon transform R of a function $f \in L_1(\mathbb{R}^n)$ is defined by a line integral over a hyperplane which is perpendicular to the direction θ with signed distance s from the origin

$$Rf(\theta, s) = R_\theta f(s) = \int_{\Theta^{\perp}} f(x + s\theta)\, \mathrm{d}x,\ s \in \mathbb{R}. \tag{2.7}$$

The X-ray transform P of a function $f \in L_1(\mathbb{R}^n)$ is defined by a line integral over a line $l(\theta, y)$ which is parallel to the direction θ and which passes through a point $y \in \Theta^{\perp}$

$$Pf(\theta, y) = P_\theta f(s) = \int_{\mathbb{R}} f(x + y\theta)\, \mathrm{d}x,\ y \in \Theta^{\perp}. \tag{2.8}$$

In two dimensions, the Radon transform and the X-ray transform differ from each other only in the parameterization, i.e. they are both defined as a line integral. In three dimensions, the Radon transform is an integral over a plane and cannot be used to model tomographic acquisition. The X-ray transform is described as a line integral for any dimension, and, therefore, is used for modeling. For the properties of the Radon

and X-ray transforms see e.g. the papers from A. Faridani (Faridani 2003) and E. T. Quinto (Quinto 2006).

The tomographic reconstruction problem in two dimensions is to find a good approximation of the function f based on Rf acquired over a unit sphere S^1. The tomosynthesis reconstruction problem is to reconstruct the function f based on Rf acquired on a restricted subset of a unit sphere S^1_θ. Uniqueness of the solution requires an infinite number of lines be measured. In practice, only a finite number of lines can be measured. Reconstruction from the limited angle data is more ill-posed than reconstruction from complete data (Quinto 1993). A unique solution exists but it is unstable. Only certain features of the object can be reconstructed.

A Singularity of the object is defined as a density jump between material μ_1 and μ_2 or a boundary between regions with different tissues, i.e. where the density function is not smooth. Following the works by T. Quinto (Quinto 1993, Quinto 2007) only some singularities can be stably reconstructed from the limited data. More specific, only those boundaries of the object can be reconstructed, which can be "seen" by the source. In other words, there must be an integral measured along a line, which is perpendicular to the singularity $\mathbf{n}$ in the current point, see Fig. 2.13a. Other singularities are called *invisible* and cannot be stably reconstructed, see Fig. 2.13b.

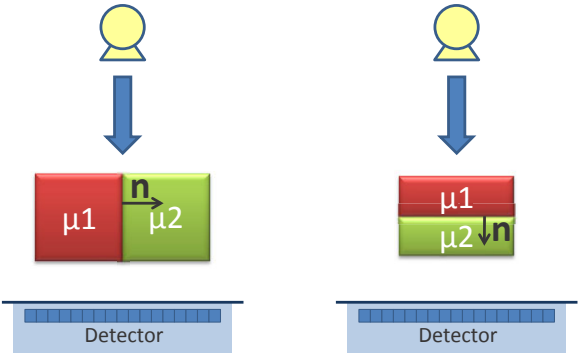

(a) visible singularity **(b)** invisible singularity

Figure 2.13: Illustration of a visible (a) and an invisible (b) singularities of an object.

Based on this principle, it can be demonstrated, which features are reconstructible in tomosynthesis. Let us consider a virtual two-dimensional phantom, which consists

of two circles, see Fig. 2.14. The fan-beam X-ray tube is moved along an arc from the position A to the position B. At each X-ray tube position, it casts two *visible* points on each circle. Based on the acquisition measured in the position A, singularities of the left sphere in points A_1 and A_2 can be reconstructed, see Fig. 2.14a. Accordingly, singularities in points B_1 and B_2 can be restored based on the acquisition from the position B. The complete movement from A to B makes singularities on circle segments A_1B_1 and A_2B_2 visible. It is important to note, that on each circle a unique set of points is visible, compare A_1B_1, A_2B_2 and A_3B_3, A_4B_4.

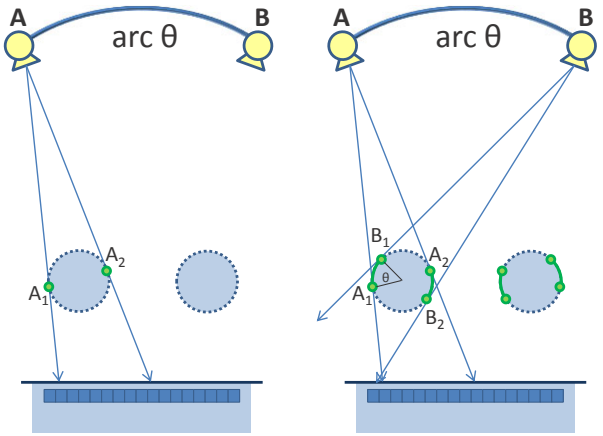

(a) Acquisition in position A **(b)** Complete acquisition from A to B

Figure 2.14: Illustration of visible and invisible singularities for a two-dimentional tomosynthesis fan-beam geometry. (a) The X-ray tube in position A makes singularities A_1 and A_2 visible. (b) The acquisition over the arc from A to B makes singularities A_1B_1 and A_2B_2 visible. Different parts of the left and the right spheres are visible.

In the three-dimensional case, the X-ray tube casts a *visible* ring on a sphere object. The orientation of visible rings depends on the position (x, y) and height z of the sphere.

2.5.3 Incomplete Fourier space

The Fourier transform is another major transform in the field of image reconstruction. The Fourier transform $\widehat{F}(\boldsymbol{\omega})$ of a real or a complex-valued n-dimensional function $f(\mathbf{x})$

is defined as the integral

$$\widehat{F}(\boldsymbol{\omega}) = \left(\frac{1}{2\pi}\right)^{\frac{n}{2}} \int_{R^n} f(\mathbf{x}) e^{-i\boldsymbol{\omega}\mathbf{x}} d\mathbf{x}, \tag{2.9}$$

and its inverse is defined as

$$f(\mathbf{x}) = \left(\frac{1}{2\pi}\right)^{\frac{n}{2}} \int_{R^n} \widehat{F}(\boldsymbol{\omega}) e^{i\boldsymbol{\omega}\mathbf{x}} d\boldsymbol{\omega}. \tag{2.10}$$

An alternative definition of the Fourier transform exists, in which the coefficient 2π is inside the exponent in the integral. This is equivalent to the definition in terms of ordinary frequency u instead of angular frequency ω

$$\widehat{F}(\mathbf{u}) = \int_{R^n} f(\mathbf{x}) e^{-2\pi i\mathbf{u}\mathbf{x}} d\mathbf{x}, \tag{2.11}$$

and its inverse is

$$f(\mathbf{x}) = \int_{R^n} \widehat{F}(\mathbf{u}) e^{2\pi i\boldsymbol{\omega}\mathbf{x}} d\mathbf{u}. \tag{2.12}$$

It is also possible to exchange the signs in front of the exponent or to introduce a coefficient only in front of one equation instead of splitting it symmetrically. Different definitions in terms of frequencies are possible because of the scaling property of the Fourier transform which states that the Fourier transform of $f(\alpha x)$ is $(1/|\alpha|)\,\widehat{F}(u/\alpha)$. More information about the Fourier transform and its properties can be found e.g. in (Papoulis 1962).

The Fourier transform is the basis for the Fourier Slice Theorem (FST) (Bracewell 1956, Merserea 1974), which states that a one-dimensional Fourier transform of measured projection data $F_1\{p(\xi)_\theta\}$ under the direction view θ lies on a line, which crosses the origin of the two-dimensional Fourier transform of the image $F_2\{f(x,y)\}_\theta$

$$F_2\{f(x,y)\}_\theta = F_1\{p(\xi)_\theta\}. \tag{2.13}$$

A schematic representation of the tomosynthesis measurement process and the filling of the Fourier space according to the FST are shown in Fig. 2.15. The tomosynthesis acquisition with an X-ray tube trajectory along an arc $\theta_x = \angle AOB$ covers only the limited wedge $\theta_x = \angle AOB = \angle A_\omega O_\omega B_\omega$ in the Fourier domain. The incompleteness of the Fourier domain results in artifacts in the reconstructed images, because information about features oriented along certain directions is unavailable.

2.5.4 Tuy-Smith sufficiency condition

Tuy and Smith independently in 1983 and 1985 derived a sufficiency condition for an object reconstruction (Tuy 1983, Smith 1985). The sufficiency condition states that one can reconstruct the object exactly if on every plane that intersects the support of the object Ω there exists at least one X-ray source point. Examples of trajectories which fulfill the condition are: two orthogonal circles, a spiral or two parallel circles connected by a line(Buzug 2008). A circular trajectory, which is usually used in micro-CT does not fulfill the conditions and neither does the tomosynthesis limited angle acquisition geometry. However, one can find some planes which fulfill the condition, compare Fig. 2.16.

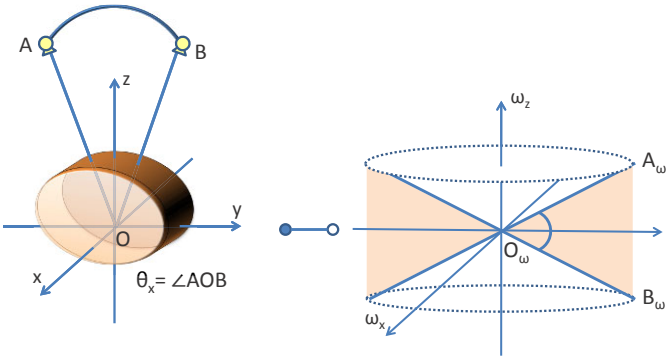

(a) image domain **(b)** Fourier domain

Figure 2.15: Illustration of the incomplete Fourier domain. Only the limited wedge $\theta_x = \angle AOB = \angle A_\omega O_\omega B_\omega$ is filled during tomosynthesis acquisition along an arc trajectory.

2.5.5 Artifacts and limited resolution

Although tomosynthesis is a volumetric imaging technique and provides dimensional information about structures, the complete three-dimensional information about the object cannot be reconstructed. As it was discussed in the previous section, the incompleteness of the tomosynthesis projection data results in a missed wedge in the Fourier space and lost singularities of the Radon transform (Quinto 1993). Furthermore, the Tuy-Smith sufficiency condition (Tuy 1983, Smith 1985) are not fulfilled. Therefore,

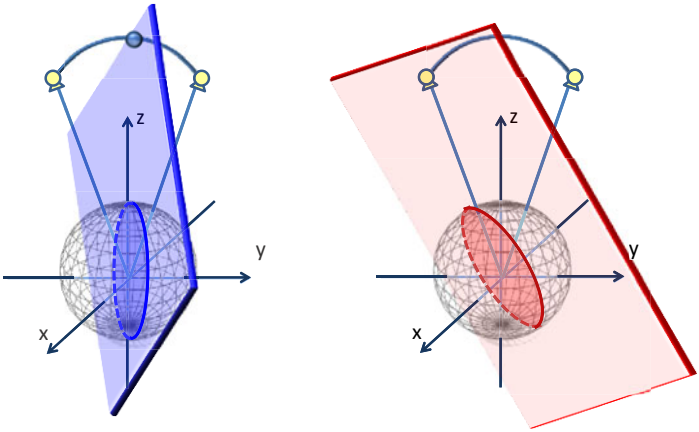

(a) plane fulfills the condition **(b)** plane does not fulfill the condition

Figure 2.16: Illustration of a plane which fulfills the Tuy-Smith sufficiency condition (a) and doesn't fullfill the condition (b) in tomosynthesis acquisition along an arc trajectory.

an accurate reconstruction in tomosynthesis is a challenging task. The incompleteness of the projection data results in artifacts and limits the axial resolution of the reconstructed volume. Thus, tomosynthesis yields images with an anisotropic resolution.

In the xy-planes artifacts corrupt the appearance of boundaries and might hide fine structures. Another appearance of limited angle artifacts is that shapes appear distorted in axial slices and features are surrounded by a sandglass-shaped halo in z-direction. It is known that the intensity and an artifact spread in z-direction is proportional to the size and density of the artifact-causing features (Svahn 2007, Reiser 2007, Hu 2008a).

One appearance of limited angle artifacts are out-of-focus artifacts (also called structural noise) which appear on the target plane and are produced by structures located above or below the current plane. The formation and propagation of such artifacts through the volume is shown in Fig. 2.17. The object is an apple with several metal needles inserted into it parallel to the detector with a 10 mm spacing. At a height of 48 mm two needles are inserted. On the two-dimensional projection image all six needles are visible, but the information about their location in z-direction is lost. The reconstructed results show that all needles are reconstructed on their correct positions, see the slice at 11 mm (Fig. 2.17c) and the slice at 48 mm (Fig. 2.17e). At the same time, strong out-of-focus artifacts are presented in the slice at 25 mm (Fig. 2.17e) as

multiple ghosting copies of needles from slices above and below.

An example of out-of-focus artifacts in clinical images of a hand is shown in Fig. 2.18b. These artifacts are highlighted by arrows. The structures in the axial slices have a distorted shape and are surrounded by a triangle-shaped halo (Fig. 2.18c).

Limited angle artifacts limit the diagnostic value of DT images. Therefore a lot of effort is made to investigate how to improve tomosynthesis performance and obtain images with better quality.

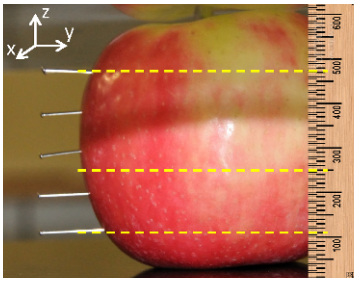

(a) an apple with metal needles

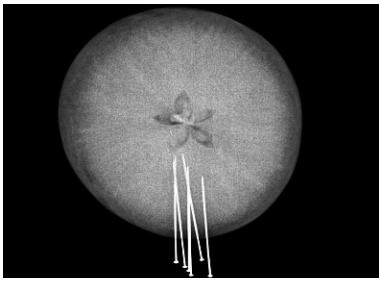

(b) projection image

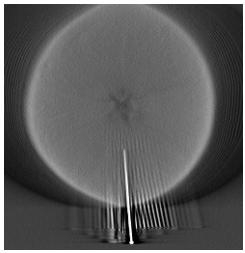

(c) slice at 11 mm, with one needle

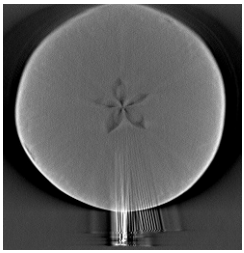

(d) slice at 25 mm, no needles

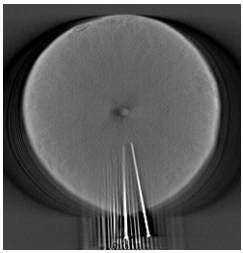

(e) slice at 48 mm, with two needles

Figure 2.17: Tomosynthesis raw-data and reconstructed slices (Siemens FBP) of an apple with five needles, 10 mm spacing. Images illustrate a propagation of the out-of-focus artifacts produced by high-attenuation objects (needles).

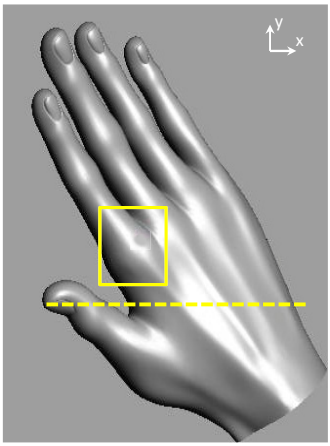

(a) selected ROIs

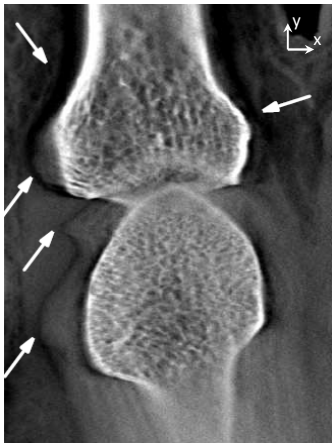

(b) in-plane appearance

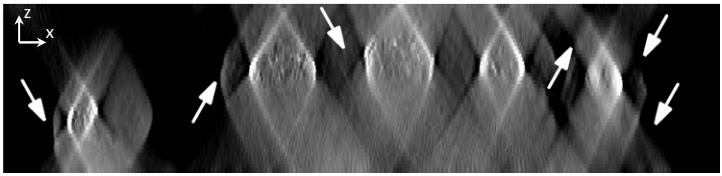

(c) axial appearance

Figure 2.18: The reconstructed volume of a hand shows artifacts in tomosynthesis. (b) in-plane appearance; (c) axial appearance

http://www.springer.com/978-3-658-05696-4

Three-Dimensional Digital Tomosynthesis
Iterative Reconstruction, Artifact Reduction and
Alternative Acquisition Geometry
Levakhina, Y.
2014, XVIII, 192 p. 71 illus., 6 illus. in color., Softcover
ISBN: 978-3-658-05696-4